Rapid and highly sensitive detection of Enterovirus 71 by using nanogold-enhanced electrochemical impedance spectroscopy

2013 Nanotechnology 24 285102

(http://iopscience.iop.org/0957-4484/24/28/285102)

Nanotechnology **24** (2013) 399501 (1pp) doi:10.1088/0957-4484/24/39/399501

Corrigendum: Rapid and highly sensitive detection of Enterovirus 71 by using nanogold-enhanced electrochemical impedance spectroscopy

2013 *Nanotechnology* **24** 285102

Hsing-Yuan Li[1,2], Shing-Hua Tseng[1], Tsai-Mu Cheng[1,3], Hsueh-Liang Chu[1], Yu-Ning Lu[1], Fang-Yu Wang[1], Li-Yun Tsai[4], Juo-Yu Shieh[5], Jyh-Yuan Yang[5], Chien-Chang Juan[6], Lung-Chen Tu[1,7] and Chia-Ching Chang[1,8]

[1] Department of Biological Science and Technology, National Chiao Tung University, Hsinchu, Taiwan
[2] Department of Pediatrics, National Taiwan University Hospital, Hsinchu Branch, Hsinchu, Taiwan
[3] The PhD Program for Translational Medicine, Taipei Medical University and Academia Sinica, Taiwan
[4] Institute of Biomedical Sciences, Academia Sinica, Taiwan
[5] Department of Health, Research and Diagnostic Center, Centers for Disease Control, Taipei, Taiwan
[6] Department of Pediatrics, National Yang-Ming University School of Medicine, Ilan branch, Taiwan
[7] Department of Plastic Surgery, Mackay Memorial Hospital, Taipei, Taiwan
[8] Institute of Physics, Academia Sinica, Taiwan

E-mail: ccchang01@faculty.nctu.edu.tw

Received 16 July 2013
Published 6 September 2013
Online at stacks.iop.org/Nano/24/399501

In figure 4 of the original published paper, the unit of *X*-axis shall be corrected to 'copy numbers/50 μl'. In order to present clearly, the color of particle size distribution of 2, 18 and 40 nm AuNPs, in the inset, are shown as green, red, and blue, respectively. The corrected version of figure 4 is presented below.

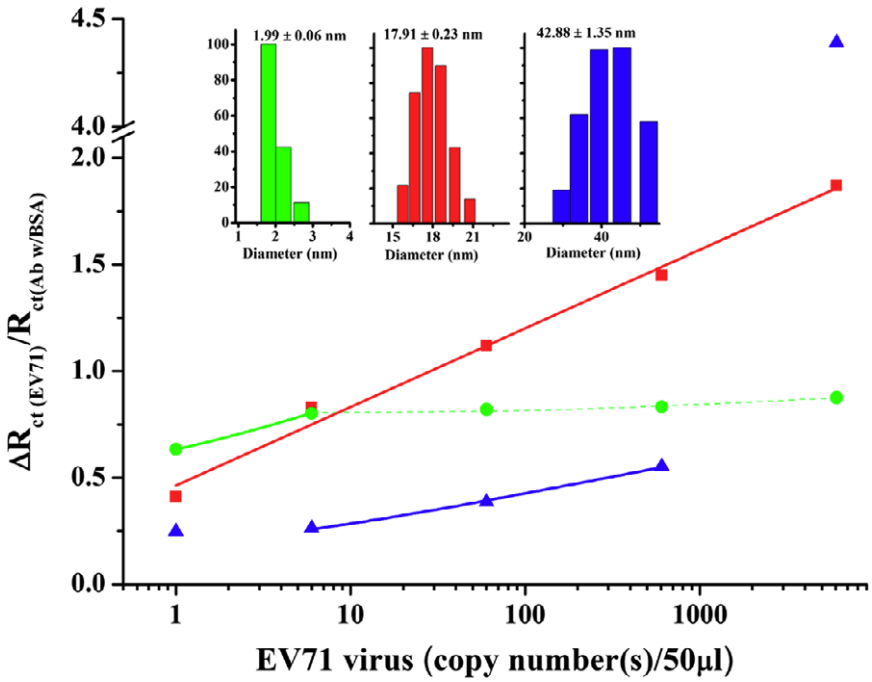

Figure 4. EV71 concentration compared with the relative change of charge transfer resistance with various sizes of AuNPs. AuNPs with sizes of 2, 18 and 40 nm are shown as green, red, and blue respectively. The lowest detection of limit of 2, 18, and 40 nm AuNPs conjugated with Anti-EV71 Ab, were 1, 1, and 61 copy number(s)/50 μl reaction volume, respectively. The linear range of 2, 18 and 40 nm AuNPs after conjugation with anti-EV71 Ab were 1–6, 1–6050 and 6–605 copy numbers/50 μl reaction volume, respectively. The 18 nm AuNPs showed the best performance in connecting anti-EV71 Ab to detect EV71. The inset denotes the particle size distributions of 2, 18 and 40 nm AuNPs by DLS measurement.

Nanotechnology **24** (2013) 285102 (9pp) doi:10.1088/0957-4484/24/28/285102

Rapid and highly sensitive detection of Enterovirus 71 by using nanogold-enhanced electrochemical impedance spectroscopy

Hsing-Yuan Li[1,2], Shing-Hua Tseng[1], Tsai-Mu Cheng[1,3], Hsueh-Liang Chu[1], Yu-Ning Lu[1], Fang-Yu Wang[1], Li-Yun Tsai[4], Juo-Yu Shieh[5], Jyh-Yuan Yang[5], Chien-Chang Juan[6], Lung-Chen Tu[1,7] and Chia-Ching Chang[1,8]

[1] Department of Biological Science and Technology, National Chiao Tung University, Hsinchu, Taiwan
[2] Department of Pediatrics, National Taiwan University Hospital, Hsinchu Branch, Hsinchu, Taiwan
[3] The Ph.D. Program for Translational Medicine, Taipei Medical University and Academia Sinica, Taiwan
[4] Institute of Biomedical Sciences, Academia Sinica, Taiwan
[5] Department of Health, Research and Diagnostic Center, Centers for Disease Control, Taipei, Taiwan
[6] Department of Pediatrics, National Yang-Ming University School of Medicine, Ilan branch, Taiwan
[7] Department of Plastic Surgery, Mackay Memorial Hospital, Taipei, Taiwan
[8] Institute of Physics, Academia Sinica, Taiwan

E-mail: ccchang01@faculty.nctu.edu.tw

Received 26 February 2013, in final form 3 May 2013
Published 20 June 2013
Online at stacks.iop.org/Nano/24/285102

Abstract
Enterovirus 71 (EV71) infection is an emerging infectious disease causing neurological complications and/or death within two to three days after the development of fever and rash. A low viral titre in clinical specimens makes the detection of EV71 difficult. Conventional approaches for detecting EV71 are time consuming, poorly sensitive, or complicated, and cannot be used effectively for clinical diagnosis. Furthermore, EV71 and Coxsackie virus A16 (CA16) may cross react in conventional assays. Therefore, a rapid, highly sensitive, specific, and user-friendly test is needed. We developed an EV71-specific nanogold-modified working electrode for electrochemical impedance spectroscopy in the detection of EV71. Our results show that EV71 can be distinguished from CA16, Herpes simplex virus, and lysozyme, with the modified nanogold electrode being able to detect EV71 in concentrations as low as 1 copy number/50 μl reaction volume, and the duration between sample preparation and detection being 11 min. This detection platform may have the potential for use in point-of-care diagnostics.

(Some figures may appear in colour only in the online journal)

1. Introduction

Enterovirus 71 (EV71) has become the most fulminant virus of the enteroviruses (EVs) after the global eradication of polio [1]. It was first identified in California in 1969 as a neurotropic virus that can cause acute flaccid paralysis, encephalitis, rhombencephalitis, neurological paralysis, myocarditis, pulmonary oedema, and death within three days of infection [2, 3]. Large outbreaks and mortality were reported in Bulgaria, Hungary, Australia, Japan, Taiwan, Singapore, Malaysia, and China [4–11]. Children with EV71 infections may present with mild respiratory tract infection, sore throat, and/or skin rash in the early stage, similar to other EV infections, in particular Coxsackie A16 (CA16) [12].

Therefore, making a definite diagnosis of EV71 infection is difficult, but is critical.

Conventional viral diagnostic procedures, such as cell culture testing, the neutralization test, and reverse transcription polymerase chain reaction (RT-PCR), have been used to investigate EV71 [13–15]. However, these virus detection procedures are expensive, slow, or complicated. Therefore, the application of these methods is appropriate for epidemiological monitoring but not for clinical diagnosis. A commercial quick strip test had been developed for the detection of EV71 and CA16 in the 1990s, but it was not clinically applicable because CA16 proved not as serious as EV71. A rapid and specific EV71 diagnostic test has not yet been developed up to the time of this study.

Electrochemical impedance spectroscopy (EIS), which measures the molecular interaction of the electrode surface, is rapid and sensitive [16]. Nanogold particles (AuNPs) can enhance the signal of EIS by increasing the surface area and reducing impedance and steric hindrance between antigen (Ag)–antibody (Ab) interaction, thus increasing the sensitivity of EIS [17, 18]. When the electrode is modified with AuNPs and a specific Ab, EIS can be an excellent tool to detect trace microorganisms. This powerful technique monitors events on sensing electrodes, and has shown promising results for point-of-care and real-time monitoring [19–21].

In this study, we investigated the effects of different interfacial self-assembled monolayer (SAM) types of working probes and found the cysteamine–glutaraldehyde–cysteamine (CGC) should be the appropriate interfacial layer for further working probe modification. Therefore, a workable nanogold-enhanced EIS probe for EV71 detection has been developed. To the best of our knowledge, EV71 detection by EIS has not been reported previously. In addition, our biosensing probe can reliably distinguish EV71 from CA16, Herpes simplex virus (HSV), and lysozyme, and the detection limit of this probe is as low as a single EV71 viral particle per reaction (50 μl of reaction volume). The entire detection process, including the Ag–Ab reaction and EIS analysis, can be completed within 11 min. In summary, we have developed a rapid, easy to perform, and highly specific and sensitive EIS platform for EV71 detection.

2. Materials and methods

2.1. Materials

Cysteamine (BioChemika grade), glutaraldehyde (Grade I), 3-mercaptopropionic acid (3-MPA), (3-mercaptopropyl)-trimethoxysilane (3-MPS), and sodium citrate were purchased from Sigma-Aldrich (St Louis, Mo, USA). Hydrogen tetrachloroaurate (III) trihydrate (ACS, 99.99%) was purchased from Alfa Aesar (Ward Hill, MA, USA). Potassium hexacyanoferrate (III) and potassium hexacyanoferrate (II) of ACS grade were purchased from J T Baker (Mallinckrodt Baker, Inc., Phillipsburg NJ, USA). Bovine serum albumin (BSA) (Biotechnology grade) was obtained from Amersco (Solon, OH, USA). Hen egg white lysozyme (BioChemika grade) was purchased from Fluka (Buchs, Switzerland). Phosphate buffered saline (PBS) at a pH of 7.4 was prepared with final concentrations of 137 mM NaCl, 10 mM phosphate, and 2.7 mM KCl. All solutions were prepared with double-distilled water (ddH_2O). Ultem 1000 (polyetherimide) was purchased from Chenway Co., Ltd (Taichung City, Taiwan). Gold wire (250 μm) of 99.99% purity was purchased from Yuh-Cheng Materials Co., LTD (Taoyuan, Taiwan). Silver wire (100 μm) and Teflon-coated platinum wire were purchased from AM System, Inc. (WA, USA). Vycor porous glass was purchased from Vycor Co. (Iserlohn, Germany). A specific anti-EV71 monoclonal Ab was purchased from Abnova (Taoyuan, Taiwan). Inactive EV71, CA16, and HSV were obtained from the Centers for Disease Control and Prevention (CDC), Taiwan, ROC. The measured viral titres of EV71, CA16, and HSV were 1.21×10^6, 3.16×10^5, 6.31×10^6 copy numbers ml^{-1}, respectively, by real-time RT-PCR.

2.2. Preparation of colloidal gold nanoparticles

The preparation of AuNPs at 2, 18 and 40 nm in size, which had been described previously, were used in this study [22, 23]. Briefly, aqueous solutions of $HAuCl_4$ (0.01%, w/v) and sodium citrate (1%, w/v) were prepared in ddH_2O. $HAuCl_4$ solution (60 ml) was boiled in a flask containing a condenser. Sodium citrate was slowly dropped into the vigorously mixing and boiling $HAuCl_4$ solution. The solution turned from light yellow to dark blue, then finally to ruby red. The solution was boiled and vigorously mixed for 30 min and then refluxed for an additional 15 min without heat. The AuNPs prepared with sodium citrate 0.9 ml and 0.3 ml using this method had average particle sizes of 18 and 40 nm, respectively [22]. The cooled AuNPs stock solution was stored at 4 °C until further use. Two nm AuNPs were produced as previous described by Bonnard [24]. The size distribution was determined by dynamic light scattering analysis [25].

2.3. Disposable working electrode modification and antibody immobilization

Modification of the working electrode and the formation of a SAM were modified from previous described methods [19, 26, 27]. Briefly, a gold electrode was polished with various grits of abrasive papers followed by aluminum oxide powders (0.3 and 0.05 μm in diameter, respectively) on microcloth pads. Next, the gold electrode was rinsed in ddH_2O and sequentially ultrasonicated in ddH_2O and absolute ethanol for 5 min each. Subsequently, the electrode was electrochemically polished in a 0.1 M H_2SO_4 solution. The electrode was polished via potential scanning from 0 to +1.6 V (versus Ag/AgCl) at a scan rate of 80 mV s^{-1} until a stable cyclic voltammogram (CV) was obtained.

2.3.1. Self-assembled monolayer selection. For comparing the SAM interfacial effect of EIS probes, three SAM processes (3-MPA, 3-MPS, and CGC), were prepared and the conductivity of the probes was tested without AuNPs by EIS.

For 3-MPA SAM formation, the polished bare gold was immersed in 0.02 M 3-MPA for 12 h [27].

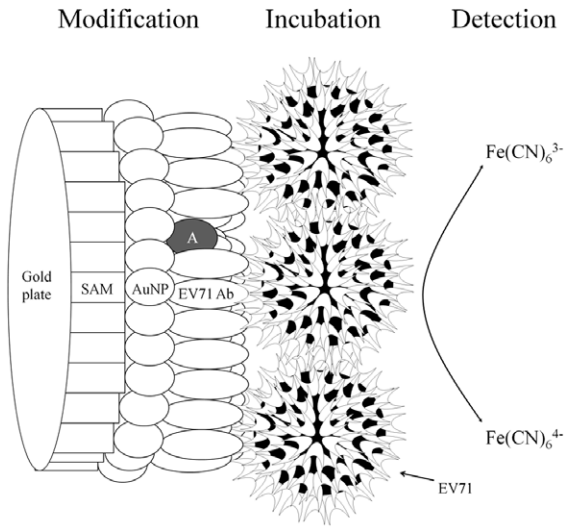

Figure 1. Scheme of the working electrode modification, antigen incubation and EIS reaction process. The working electrode was modified with SAM, AuNPs, EV71 Ab and BSA (A). The EV71 sensing probe was immersed in EV71 samples. After washing with PBS, the probe was tested by EIS with the electrolyte of hexacyanoferrate ($Fe(CN)_6^{3-/4-}$). (SAM may be modified by a CGC, 3-MPA, or 3-MPS layer. In this study, the CGC layer was chosen for further study.)

For 3-MPS SAM formation, the polished bare gold was immersed in 40 mM 3-MPS in methanol for 3 h. The silane units were polymerized by dipping into aqueous 0.01 M NaOH for 2 h [28].

For CGC SAM formation, following the electrochemical polish the gold electrode was rinsed with ddH_2O and immersed in a 20 mM cysteamine aqueous solution for 12 h. After removing the physically adsorbed cysteamine with copious amounts of ddH_2O, the electrode was modified by soaking in a glutaraldehyde solution (12.5%, v/v) for 1 h. Subsequently, the electrode was rinsed with ddH_2O and soaked in a 20 mM cysteamine solution for approximately 12 h before it was rinsed again with ddH_2O.

2.3.2. Nanogold conjugation and antibody immobilization. After the SAM was formed, the electrode was immersed immediately in 50 μl of various sizes of AuNPs for 12 h and then covered with a monolayer of AuNPs. The modified electrode was soaked in anti-EV71 Ab (50 μl, 1 μg ml^{-1} in 1× PBS, pH 8.8) at 4 °C for approximately 12 h and rinsed with PBS (pH 7.4) to thoroughly remove the excess particles physically adsorbed on its surface. Furthermore, the electrode was immersed in BSA solution (10 mg ml^{-1}) for 30 min to block nonspecific binding sites of the AuNPs. The scheme highlighting the sequential connection of the compounds on the working electrode is shown in figure 1. All electrodes were washed again with PBS (pH 7.4) and stored at 4 °C until use.

2.4. Electrochemical measurements

All electrochemical measurements were performed with a three-electrode cell. These electrodes included a modified Au electrode (working electrode), a coiled platinum wire (counter-electrode), and an Ag/AgCl wire immersed in 3 M KCl (reference electrode). All experiments were performed at room temperature, and all potentials in this work were measured with direct relevance to the Ag/AgCl reference electrode. The EIS operates with a 10 mV AC sinusoidal amplitude and a 0.23 V (versus Ag/AgCl) direct current (DC) potential, which is the standard oxidizing potential of 2.5 mM $Fe(CN)_6^{4-/3-}$ (1:1 in 10 mM PBS solution [pH 7.4]), and a frequency ranging from 1 to 10^5 Hz. $Fe(CN)_6^{4-/3-}$ acted as a redox substance in this study. ZSimpWin V 3.20 software from Informer Technologies Inc. (Tennessee, USA) was used for simulation to reveal the related electrical parameters of the working electrode. The working electrode is disposable after using once. Each diluted sample was detected three times with different working probes. The parameters of the Nyquist plot were calculated using ZSimpWin V 3.20 and shown as mean ± standard deviation (SD).

The impedance between the working electrode and the counter-electrode can be represented as a modified Randles circuit, which is properly applied under semi-infinite conditions. The parameters of a modified Randles circuit include the resistance of solution (R_{sol}), the constant phase element (Q), the charge transfer resistance (R_{ct}), and the Warburg element (W). R_{sol} is an active electrolyte resistance between the work electrode and the counter-electrode. Q is the behaviour of a double layer of the working electrode, which is usually an imperfect capacitor. The formula for calculating the imperfect Q is the following:

$$Q = \frac{1}{Q_0}(j\omega)^{-n},$$

where Q_0 is capacitance, j is the imaginary unit, ω is the angular frequency and n is a number between 0 and 1. When $n = 1$, Q is an ideal capacitor; when $n = 0$, Q is a pure resistor.

R_{ct} and W are defined as the active charge transfer resistance and the specific electrochemical element of diffusion of the impedance of a Faradaic reaction, respectively. The relative charge transfer resistance ratio ($\Delta R_{ct(Analyte)}/R_{ct(Ab\ (BSA))}$) is adopted because of its relationship to the concentration of EV71.

2.5. Sample preparation

The viruses were diluted with PBS in a series of ten-fold dilutions to evaluate the detection limits of our method. The lysozyme was diluted with PBS serially ten-fold to a concentration of 1 nM–1 mM. Fifty microlitres of analytic samples were incubated for 10 min.

3. Results

3.1. Self-assembled monolayer selection

There are many type of SAMs applied as the interface-layer in biosensors, such as CGC, 3-MPA, and 3-MPS [21, 27, 28]. The detection range may be affected by the conducting

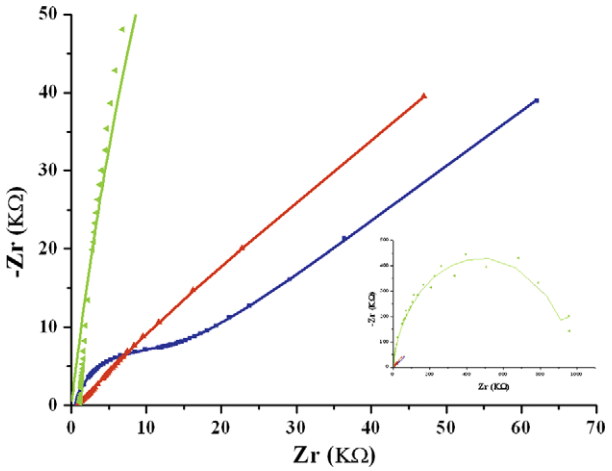

Figure 2. Conductivity of various SAMs determined by EIS. Red line: CGC SAM; blue line: 3-MPA SAM; green line: 3-MPS SAM. The R_{ct} simulated by Randles model, of 3-MPA, 3-MPS and CGC SAMs are 0.7, 7.9 kΩ, and 964.4 kΩ, respectively.

feature of the SAM layer. Figure 2 shows the Nyquist plot of different SAMs determined by EIS. The R_{ct} of CGC, 3-MPA, and 3-MPS were 0.7, 7.9, and 964.4 kΩ, respectively. Figure 2 shows the conductivities of various SAMs, indicating that the CGC SAM has the lowest resistance and is therefore the most appropriate connecting interfacial layer for the detection of low EV71 concentrations. Additionally, the thiol tail can connect to AuNPs, which can enhance the signal by increasing surface area. Therefore, the CGC SAM was used in the subsequent study.

3.2. Verification and characterization of the working electrode via cyclic voltammetry

Figure 3(a) shows the working electrode chemical polish in 0.1 M H_2SO_4 with the potential 0–1.6 V (versus Ag/AgCl). The positive sweep peaks are 1.085 V and 1.261 V (versus Ag/AgCl), respectively. The negative sweep peaks are 0.937 V and 0.775 V (versus Ag/AgCl), respectively. The cleanliness and purity of the gold plate are consistent with Kondo and Burke [29, 30].

Each step of the surface-modified working electrode was verified with CV during the biosensor electrode preparation and is shown in figure 3(b). The CV responses of the electrode in various modification stages were measured in 2.5 mM $K_3Fe(CN)_6/K_4Fe(CN)_6$ redox electrolyte in PBS (pH 7.4) with a scan rate of 80 mV s^{-1} between −0.2 and +0.6 V (versus Ag/AgCl). In the bare Au electrode state, a reversible CV with peak-to-peak current amplitude (ΔI_p) of 735.22 nA was obtained. When the bare Au electrode was modified with the CGC layers, ΔI_p of the CGC/Au redox electrode decreased to 701.82 nA. Furthermore, when the 18 nm AuNPs were chemically bound to the CGC/Au electrode (denoted as AuNPs/CGC/Au), ΔI_p became 719.99 nA. ΔI_p decreased to 495.76 nA when the AuNPs/CGC/Au electrode was linked with anti-EV71 Ab and BSA, which bound the probe surface where the anti-EV71 Ab was not conjugated (Ab(BSA)/AuNPs/CGC/Au). The CVs of

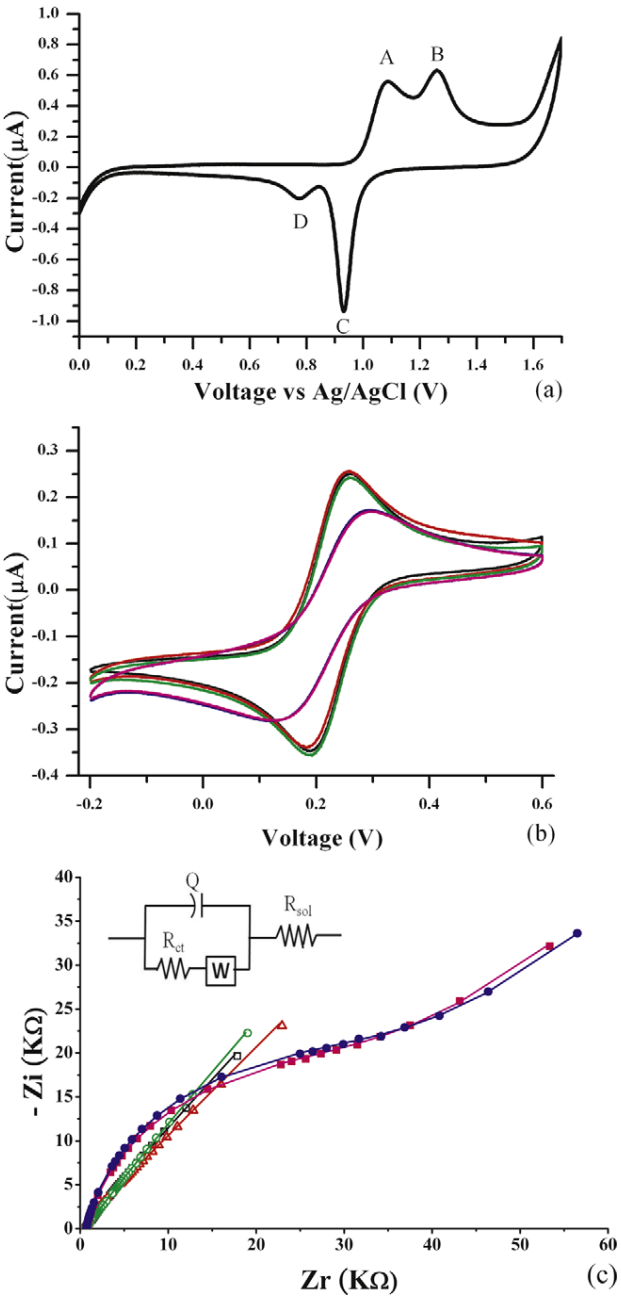

Figure 3. (a) The cyclic voltammetry of bare gold in 0.5 M H_2SO_4. Peak A: oxidation of Au (100); peak B: oxidation of Au(111); peak C: reduction of Au(100) and Au(111); peak D: reduction of the multilayer of Au. (b) The cyclic voltammetry of working electrode modifications. Black line: bare gold of the electrode; green line: CGC/Au; red line: AuNPs/CGC/Au; pink line: EV71 Ab/AuNPs/CGC/Au; blue line: EV71 Ab(BSA)/AuNPs/CGC/Au. (c) Nyquist plot of the working electrode modification and modified Randles circuit. Black line: bare gold; green line: CGC/Au; red line: AuNPs/CGC/Au; pink line: EV71 Ab/AuNPs/CGC/Au; blue line: EV71 Ab(BSA)/AuNPs/CGC/Au. All dots represent raw data, and all lines are simulated by ZSimpWin V 3.20 software. The inserted scheme shows the Randles circuit. R_{sol}: resistance of electrolyte in mass solution; R_{ct}: charge transfer resistance; Q: constant phase element of non-infinite solution; W: Warburg element.

various modification stages of gold electrode showed that ΔI_p decreased gradually when the electrode was modified sequentially with CGC, AuNPs, Ab and BSA (figure 3(b)).

Table 1. Stimulation of the Nyquist plot for the working electrode modifications ($n = 3$).

	Bare gold	C–G–C	AuNP	EV71 Ab	BSA
R_{ct} (kΩ)	0.27 ± 0.03	0.87 ± 0.04	1.30 ± 0.08	30.56 ± 5.02	34.83 ± 1.79
Q (μS s^{-n})	0.05 ± 0.04	0.20 ± 0.25	0.25 ± 0.23	0.10 ± 0.06	0.07 ± 0.02
n	0.96 ± 0.05	0.86 ± 0.12	0.83 ± 0.09	0.82 ± 0.04	0.87 ± 0.01
W (μS $s^{-1/2}$)	4.04 ± 0.57	3.68 ± 0.15	3.66 ± 0.27	2.91 ± 0.27	3.83 ± 0.18
R_{sol} (kΩ)	0.59 ± 0.02	0.63 ± 0.05	0.63 ± 0.01	0.64 ± 0.02	0.52 ± 0.05
ChiSq ($\times 10^{-4}$)	3.97 ± 0.77	3.94 ± 0.95	4.66 ± 0.27	7.40 ± 0.35	5.16 ± 0.85

The peak-to-peak voltage of the working electrode also showed the property change when the working electrode was modified with biological substances. The peak-to-peak voltage (ΔE) of bare gold was 72.68 mV. The ΔE values of CGC/Au, AuNPs/CGC/Au, and Ab (BSA)/AuNPs/CGC/Au were 75.05, 65.33, and 179.8 mV, respectively. ΔE increasing and ΔI_p decreasing progressively indicated the high resistance substance conjugated on the probe systematically during probe modification.

The Nyquist plot and the parameters of EIS for working probe modification are shown in figure 3(c) and table 1, respectively. As the EIS parameter is derived from the Nyquist plot, the charge transfer resistance (R_{ct}) yields the most suitable data for evaluating the electrode surface reference, a value that is correlated to the change in peak-to-peak amplitude of CV. The R_{ct} of EIS increased as the peak-to-peak amplitude decreased. The R_{ct} values of bare gold, CGC/Au, AuNPs/CGC/Au, and Ab(BSA)/AuNPs/CGC/Au were 0.27 ± 0.03, 0.87 ± 0.04, 1.30 ± 0.08 and 34.83 ± 1.79 kΩ, respectively. After modification with Ab, the R_{ct} value of the probe changes considerably. This indicates that R_{ct} is more sensitive when the probe is conjugated with large bio-substances than with small chemicals.

3.3. Effect in sensitivity of the working probe with different sizes of AuNPs

As indicated in previous studies, the AuNPs may enhance the signal of EIS and reduce the steric hindrance between the Ag and Ab interaction [17, 18]. It is interesting to study the size effect of AuNPs-modified probes. Figure 4 demonstrates EV71 detection limits and a linear range between 1 and 6050 copy numbers/50 μl reaction volume with different sizes of AuNPs. Figure 4 inset shows the size analysis of AuNPs by DLS. The sizes of the 2, 18, and 40 nm AuNPs were measured as 1.99 ± 0.06 nm, 17.91 ± 0.23 nm and 42.88 ± 1.35 nm. As the threshold of ΔR_{ct} is 0.38, the detection of limits of 2, 18, and 40 nm nanogold-enhanced working probes were 1, 1 and 61 copy number(s)/50 μl reaction volume. The linear ranges of 2, 18, and 40 nm nanogold-enhanced probes were 1–6, 1–6050, and 6–605 copy numbers/50 μl reaction volume, respectively. These results showed the working probes with 18 nm AuNPs show the lowest detection limit and the widest linear range in our modification protocol. However, working probes with 2 and 40 nm AuNPs modifications did not have a similar enhanced ability. Therefore, 18 nm AuNPs were used in the following study.

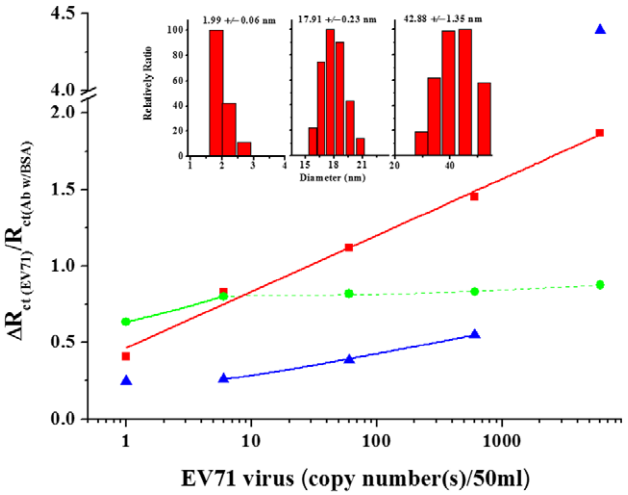

Figure 4. EV71 concentration compared with the relative change of charge transfer resistance with various sizes of AuNPs. AuNPs with sizes of 2, 18 and 40 nm are shown as green, red, and blue respectively. The lowest detection of limit of 2, 18, and 40 nm AuNPs conjugated with Anti-EV71 Ab, were 1, 1, and 61 copy number(s)/50 μl reaction volume, respectively. The linear range of 2, 18 and 40 nm AuNPs after conjugation with anti-EV71 Ab were 1–6, 1–6050 and 6–605 copy numbers/50 μl reaction volume, respectively. The 18 nm AuNPs showed the best performance in connecting anti-EV71 Ab to detect EV71. The inset denotes the particle size distributions of 2, 18 and 40 nm AuNPs by DLS measurement.

3.4. Incubation time and working probe performance with 18 nm AuNPs

To determine the optimal incubation time, the incubation time versus the ratio of the change of R_{ct} is plotted in figure 5. As shown, there were no obvious differences in the $\Delta R_{ct(Ag)}/R_{ct(Ab\ w/BSA)}$ ratio after incubation for 3 min, and it reached a plateau after incubation for 10 min. For higher sensitivity, the analyte was incubated for 10 min in this study.

CA16, HSV, and lysozyme were used to test the binding specificity of EV71 electrodes. The relative charge transfer resistance ratio of various concentrations of EV71, CA16, HSV and lysozyme are shown in figure 6. The data plotted as $\Delta R_{ct(Analyte)}/R_{ct(Ab(BSA))}$ reflect the relative increase of charge transfer resistance compared with $R_{ct(Ab(BSA))}$, where $R_{ct(Ab(BSA))}$ represents the baseline of charge transfer resistance when the Ab-immobilized electrode was immersed in EV71-free solution. The data showed no obvious change in lysozyme (1 nM–1 mM), HSV (3.15–3.15 × 10^4 copy numbers/50 μl reaction volume) and CA16

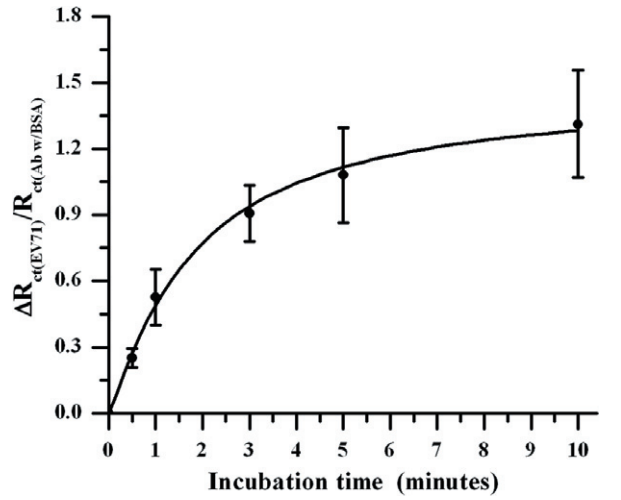

Figure 5. The different incubation times of 61 copy numbers/50 μl reaction volume of EV71 compared with the relative change of charge transfer resistance.

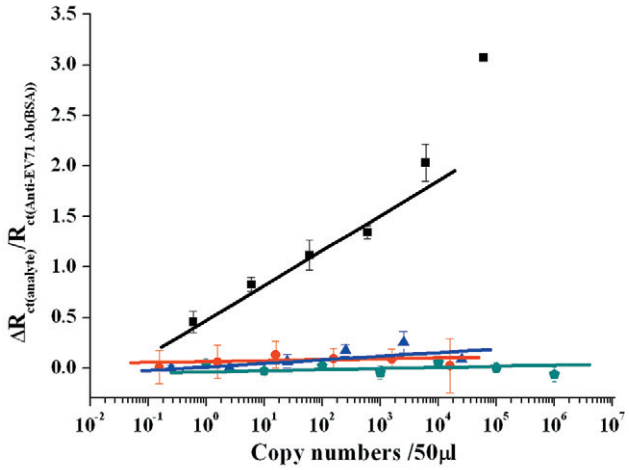

Figure 6. Analyte concentration compared with the relative change of charge transfer resistance with 18 nm AuNPs. Ten-fold serial dilutions of EV71, CA16, HSV, and lysozyme compared with the relative charge transfer resistance. Black line: EV71; blue line: CA16; red line: HSV; green line: lysozyme. (For lysozyme, the *x*-axial unit is nM; the error bar in the scheme is SD.)

(1.58–1.58 $\times$ 10^5 copy numbers/50 μl reaction volume). The probe could detect EV71 in a concentration range between 1 and 6.05 $\times$ 10^4 copy numbers/reaction. The means of maximal $\Delta R_{ct(Analyte)}/R_{ct(Ab\,w/BSA)}$ ratio for HSV, CA16 and lysozyme were 0.17, 0.24, and 0.14, respectively. The mean value of $\Delta R_{ct(Analyte)}/R_{ct(Ab(BSA))}$ for EV71 at a concentration of 1 copy numbers/50 μl reaction volume was 0.45, which was much higher than the corresponding values for CA16, HSV or lysozyme (figure 6).

3.5. The sensitivity and specificity of the working probe

Table 2 shows the EV71 test positive and negative findings in this experiment. When the threshold was 0.45 (mean of 1 copy number/50 μl reaction volume), the sensitivity and specificity were 94% and 100%, respectively (table 2(a)). When the threshold was 0.38, both the sensitivity and specificity were 100% (table 2(b)). The appropriate threshold of ΔR_{ct} was 0.38.

Table 2. Sensitivity and specificity of the EV71 sensing probe. The thresholds of ΔR_{ct} are 0.45 and 0.38 in tables (a) and (b), respectively. (P: positive; N: negative; T: total; others include tests of 3 PBS, 21 CA16, 18 HSV and 21 lysozyme.)

		Truth		
		EV71 virus	Others	T
(a)				
EIS test	P	17	0	17
	N	1	63	64
	T	18	63	
Sensitivity = 17/18 = 94%				
Specificity = 63/63 = 100%				
(b)				
EIS test	P	18	0	18
	N	0	63	63
	T	18	63	
Sensitivity = 18/18 = 100%				
Specificity = 63/63 = 100%				

4. Discussion

In order to obtain the highest sensitivity of the EIS measurement (the R_{ct} ratio between Ag and Ab binding), the resistance of the interfacial layer between bare gold and AuNP should be as low as possible. As indicated in section 3.1 and figure 2, the CGC SAM had the lowest resistance and reduced the interference of the R_{ct} of Ab and Ag–Ab. Therefore, CGC is the best interface for further working probe modifications for detecting small amounts of particles in this study.

As shown in figure 4, the detection limits of 2 and 18 nm AuNPs have higher sensitivity as 1 copy number/50 μl reaction volume. This can be explained as the ratio of charge density in small AuNPs being higher than for larger ones. As indicated in the introduction, the AuNPs could enhance the signal of EIS by increasing the surface area and avoiding the steric hindrance [17, 18]. AuNPs of size 40 nm showed a higher detection limit and a shorter linear range than the 18 nm AuNPs modified probe. Therefore, the difference of the detection linear range may be attributed to avoiding steric hindrance through a curvature effect of the AuNPs. Accordingly, 18 nm is the appropriate size of AuNP in this study.

Electrochemistry provides an effective way to analyse the properties of surface layers [31]. The surface conformation and cleanliness of the polycrystalline gold electrode are very important for CV and EIS measurements. In CV of sulfuric acid, the straight lines from 0.2 to 0.7 V (versus Ag/AgCl) indicate that the gold surface is very clean and that no reduction or oxidation of the bare gold surface occurs during the sweep. Kondo *et al* [29] measured redox peaks of +1.3 and +0.91 V for a single crystal of Au(111) and +1.11 and

+0.93 V for a single crystal of Au(100) in 0.5 M H_2SO_4 using CV and the values were measured against an Ag/AgCl reference electrode, which is similar to what we did. In our results, the three similar redox peaks (figure 3(b), peaks A–C) indicated that most gold atoms belong to Au(111) and Au(100), showing that our electrode had the ability to form SAM [29]. The reduction peak D of 0.775 V (versus Ag/AgCl) is assigned as a multilayer oxide and/or involved hydroxide [30]. The cyclic voltammogram can characterize the interface of the working electrode. In our study, the ΔE_p of bare gold was 72.68 mV. It is higher than 59.1 mV in an ideal system by the Nernst equation, but it is consistent with Mohadesi's report [32]. Additionally, the values of I_{pa}/I_{pc} and ΔE from CV of $Fe(CN)_6^{3-/4-}$, and Q and n of bare gold from EIS indicate that the cleanliness of the gold plate surface is optimal.

Electrochemistry can also provide an effective way to analyse the properties of adsorbed layers [31]. In the CV of $Fe(CN)_6^{3-/4-}$, ΔI_p will decrease and ΔE will increase when bare gold is modified step by step with biochemical substances because the resistance of the bio-substance connected to the working probe is higher than bare gold. In our study, the R_{ct} increased when the working electrode was modified with CGC, AuNPs, and EV71 Ab and connected with EV71 sequentially, indicating a successful systematic surface modification and optimal detection. After AuNPs modification, ΔE_p was 65.33 mV, which is close to the ideal system (59.1 mV). The decreased $\Delta E_{p(AuNPs)}$ indicates the purity of the AuNPs surface, which may enhance protein chemical binding. The increased $\Delta I_{p(AuNPs)}$ might indicate an increased surface area of the working electrode. When EV71 Ab is bound to the probe, ΔI_p decreased and ΔE increased dramatically (figure 3(b)). The dramatic change of ΔR_{ct} between AuNPs and EV71 Ab-modified probes indicates that the bio-molecular size and the net negative charge of the protein might play a role in the change of resistance.

The equivalent circuit elements of a modified Randles model were applied in EIS measurement (figure 3(c) inset). The value of R_{ct}, which presents the charge transfer from the electrode during the Faradaic reaction, is the optimal parameter of the elements to analyse the Ag–Ab reaction of the working electrode in the Randles circuit. The nonhomogeneous surface of each probe would limit the application of EIS for routine clinical detection [21]. However, as indicated in the previous description, the relative charge transfer resistance ratio ($\Delta R_{ct(Analyte)}/R_{ct(Ab\ w/BSA)}$) can solve this problem and has been applied in previous studies [22].

The anti-EV71 Ab chosen in this study is specific to EV71 only. The detection limit is as high as picograms to femtograms and is used for western blot analysis. In addition, the ratio of $\Delta R_{ct(Analyte)}/R_{ct(Ab(BSA))}$ remained almost constant after the probe was immersed in serial dilutions of CA16, HSV, and lysozyme (figure 6). In summary, the EV71 sensing probe is specific to EV71 viral particles and does not interact with CA16, which shares highly sequential similarity with EV71, and HSV, which shows the similar symptoms and signs of the enterovirus [33] (figure 6). Additionally, the EV71 Ab does not interact with lysozyme (figure 6). Since the surface charge of lysozyme is positive, we can exclude the artefact of charge attraction from the working electrode probe. These results indicate that this sensor is specific to EV71, and that the EV71 sensing probe has the potential to differentiate EV71-infected children from others.

Our previous study demonstrated that the haptoglobin (Hp) detection probe can distinguish phenotypes within 1–3 nm of each other and can quantify accurately down to picomolar levels of Hp 2–2, where the molecular size and weight are 13 nm and 190 kDa respectively [21]. EV71 is an icosahedral structure consisting of 60 copies of four capsid proteins. One of the capsid proteins, virus protein 1 (VP1), is the protein detected by our probe. EV71 is 30 nm in size and 5400 kDa (not including RNA). Our virus particle is more compact than Hp, and therefore the detection limit of the EV71 diagnostic platform is better than that of the Hp diagnostic platform. In order to avoid the steric hindrance of Ag–Ab binding on the working electrode, AuNPs were used to enhance the detection signal, as described in section 1 [17, 18]. Therefore, the detection limit of EV71 can be pushed to a single viral particle, which is more sensitive than the conventional detection process.

Although the sensitivity and specificity of diagnostic tools are important in the clinic, the timing is crucial for diagnosis of severe diseases. Our study included an incubation time of 10 min, with the ΔR_{ct} being saturated and having reached a plateau (figure 3). The EIS procedure was completed within 1 min. Therefore, the total testing time is approximately 11 min, which makes the test ideal for applications in emergency rooms (ERs) or outpatient departments (OPDs). Because the EV71 sensing probe does not interact with lysozyme, the sample could be taken from an oral swab, which is less invasive than a blood sample. At the same time, this method might be convenient for doctors and acceptable for children. To avoid contaminating the operator and the environment, the probe was designed to be disposable.

In spite of important clinical application issues, our study also demonstrates that the electrochemical method is more convenient, inexpensive, and rapid than previous approaches, which include viral RNA extraction and PCR amplification, viral isolation and culture, the neutralization test and the detection of anti-EV71 IgM [34]. Viral RNA must be extracted by reagents or commercial kits and PCR amplified using a thermocycler, the settings of which are usually too complicated to be used in a clinical context. Additionally, the PCR products need further analysis by electrophoresis. The total procedure is costly, complicated, and both labour and time consuming. Viral isolation and culture requires special instruments and cell lines. When a cytopathic effect is noted, it still needs further RT-PCR amplification and sequencing to distinguish the highly similar sequences among the EV family. The neutralization test requires expensive equipment, including microtitre plates, an incubator, microscopes, and a human embryo rhabdomyosarcoma cell-line. The results are often varied because the data are collected 2–7 days after incubation. The anti-EV71 IgM detection method, which is relatively convenient, catches the μ-chain of IgM by

enzyme-linked immunosorbent assay (ELISA), and has the potential to be used in the clinic. However, ELISA needs an incubation of at least 1 h and the procedure is more complicated than our EIS approach. Additionally, detection of anti-EV71 IgM method cannot give information regarding the viral particle. In our study, the relative charge transfer resistance ratio was linear to EV71 concentrations from 1 to 6050 copy numbers/50 μl reaction volume. The quantity of EV71 particles in the patient sample may link to the viral pathogenesis, prognosis, and its ability to transmit. Therefore, this EV71-specific probe could be used for early detection of suspected carriers and infected children and for following up patients in their convalescent stage. It is known that EV71 can be transmitted by contaminated fomites, such as toys, foods, water, and household persons who contact EV71-infected patients. Our sensing probe could detect EV71 in human body fluids and environmental samples. Namely, this detection platform could effectively screen out EV71-infected/carried persons and prevent this disease becoming widespread.

In Taiwan, neurological complications and/or deaths due to EV71 infection have been reported almost every year, and large outbreaks have been reported every 3–5 years. Since 1998, thousands of children in Taiwan have contracted EV71 infection and suffered neurological sequelae and/or death [2]. Early detection of EV71 can prevent the virus spreading and monitor the disease prognosis, which can save both socioeconomic and medical costs.

5. Conclusion

There are outbreaks of EV infection in the West-Pacific region every year. Early detection of EV71 infection is needed in these countries to deploy preventive measures and may help to reduce morbidity and mortality due to EV71 infection. In this study, we demonstrate a highly sensitive and specific method that can detect EV71 in concentrations as low as approximately 1 copy number/reaction in 11 min. The simple, rapid, and highly sensitive method described in this study provides a crucial improvement for the early detection of EV71 infection, which may save many EV71-infected children.

Acknowledgments

This project was supported by NSC grant 100-2112-M-009-004-YM3, the ATU-MOE Project, Taiwan, ROC, and an internal grant from National Taiwan University Hospital HsinChu Branch (HCH100-006).

References

[1] Bible J M *et al* 2007 Genetic evolution of Enterovirus 71: epidemiological and pathological implications *Rev. Med. Virol.* **17** 371–9
[2] Chang L Y *et al* 2007 Neurodevelopment and cognition in children after Enterovirus 71 infection *N. Engl. J. Med.* **356** 1226–34
[3] Lin K H *et al* 2006 Evolution of EV71 genogroup in Taiwan from 1998 to 2005: an emerging of subgenogroup C4 of EV71 *J. Med. Virol.* **78** 254–62
[4] Chumakov M *et al* 1979 Enterovirus-71 isolated from cases of epidemic poliomyelitis-like disease in Bulgaria *Arch. Virol.* **60** 329–40
[5] Nagy G *et al* 1982 Virological diagnosis of Enterovirus type-71 infections—experiences gained during an epidemic of acute CNS diseases in Hungary in 1978 *Arch. Virol.* **71** 217–27
[6] Gilbert G L *et al* 1988 Outbreak of Enterovirus-71 infection in Victoria, Australia, with a high-incidence of neurologic involvement *Pediatr. Infect. Dis. J.* **7** 484–8
[7] Ishimaru Y *et al* 1980 Outbreaks of hand, foot, and mouth-disease by Enterovirus 71—high-incidence of complication disorders of central nervous-system *Arch. Dis. Child.* **55** 583–8
[8] Ho M T *et al* 1999 An epidemic of Enterovirus 71 infection in Taiwan *N. Engl. J. Med.* **341** 929–35
[9] Singh S *et al* 2002 Direct detection of Enterovirus 71 (EV71) in clinical specimens from a hand, foot, and mouth disease outbreak in Singapore by reverse transcription-PCR with universal Enterovirus and EV71-specific primers *J. Clin. Microbiol.* **40** 2823–7
[10] AbuBakar S *et al* 1999 Identification of Enterovirus 71 isolates from an outbreak of hand, foot and mouth disease (HFMD) with fatal cases of encephalomyelitis in Malaysia *Virus Res.* **61** 1–9
[11] Yang F *et al* 2001 The complete genome of Enterovirus 71 China strain *Sci. China Ser. C-Life Sci.* **44** 178–83
[12] Chen T C *et al* 2006 Combining multiplex reverse transcription-PCR and a diagnostic microarray to detect and differentiate Enterovirus 71 and Coxsackievirus A16 *J. Clin. Microbiol.* **44** 2212–9
[13] Shahmahmoodi S *et al* 2008 First detection of Enterovirus 71 from an acute flaccid paralysis case with residual paralysis in Iran *J. Clin. Virol.* **42** 409–11
[14] Lin T Y *et al* 2003 Proinflammatory cytokine reactions in Enterovirus 71 infections of the central nervous system *Clin. Infect. Dis.* **36** 269–74
[15] Yan J J *et al* 2001 Complete genome analysis of Enterovirus 71 isolated from an outbreak in Taiwan and rapid identification of Enterovirus 71 and Coxsackie virus A16 by RT-PCR *J. Med. Virol.* **65** 331–9
[16] Bogomolova A *et al* 2009 Challenges of electrochemical impedance spectroscopy in protein biosensing *Anal. Chem.* **81** 3944–9
[17] Su B L *et al* 2010 Thionine/nanogold multilayer film for electrochemical immunoassay of alpha-fetoprotein in human serum using biofunctional double-codified gold nanoparticles *Anal. Methods-UK* **2** 1702–9
[18] Suni I I 2008 Impedance methods for electrochemical sensors using nanomaterials *Trac.-Trend Anal. Chem.* **27** 604–11
[19] Hou Y *et al* 2007 A novel detection strategy for odorant molecules based on controlled bioengineering of rat olfactory receptor I7 *Biosens. Bioelectron.* **22** 1550–5
[20] Yanga G J *et al* 2009 A reusable capacitive immunosensor for detection of Salmonella spp. based on grafted ethylene diamine and self-assembled gold nanoparticle monolayers *Anal. Chim. Acta* **647** 159–66
[21] Cheng T M *et al* 2011 Human haptoglobin phenotypes and concentration determination by nanogold-enhanced electrochemical impedance spectroscopy *Nanotechnology* **22** 245105
[22] Grabar K C *et al* 1995 Preparation and characterization of Au colloid monolayers *Anal. Chem.* **67** 735–43
[23] Schneider G and Decher G 2008 Functional core/shell nanoparticles via layer-by-layer assembly. Investigation of the experimental parameters for controlling particle aggregation and for enhancing dispersion stability *Langmuir* **24** 1778–89

[24] Bonnard C, Papermaster D S and Kraehenbuhl J-P 1984 *Immunolabelling for Electron Microscopy* ed J M Polak and I M Varndell (New York: Elsevier) pp 95–111
[25] Svanidze A V *et al* 2012 Specific features of the temperature behavior of lysozyme diffusivity in solutions with different protein concentrations *J. Mol. Liq.* **168** 7–11
[26] Wang S Y *et al* 2007 Positive selection of hepatitis delta antigen in chronic hepatitis D patients *J. Virol.* **81** 4438–44
[27] Dong S J and Li J H 1997 Self-assembled monolayers of thiols on gold electrodes for bioelectrochemistry and biosensors *Bioelectrochem. Bioenerg.* **42** 7–13
[28] Tang D Q, Tang D Y and Tang D P 2005 Construction of a novel immunoassay for the relationship between anxiety and the development of a primary immune response to adrenal cortical hormone *Bioprocess Biosyst. Eng.* **27** 135–41
[29] Kondo T *et al* 2007 Structure of Au(111) and Au(100) single-crystal electrode surfaces at various potentials in sulfuric acid solution determined by *in situ* surface x-ray scattering *J. Phys. Chem.* C **111** 13197–204
[30] Burke L D and Nugent P F 1997 The electrochemistry of gold: I the redox behaviour of the metal in aqueous media *Gold Bull.* **30** 43–53
[31] Lai L J *et al* 2009 Surface characterization of immunosensor conjugated with gold nanoparticles based on cyclic voltammetry and x-ray photoelectron spectroscopy *Colloids Surf.* B **68** 130–5
[32] Mohadesi A, Karimi M A and Pourfarsi M 2011 A new negative charged self-assembled monolayer for selective electroanalytical determination of dopamine in the presence of ascorbic acid *Inter. J. Electrochem. Sci.* **6** 309–16
[33] Wu T C *et al* 2007 Immunity to a virulent Enterovirus 71 and Coxsackie A16 virus protects against Enterovirus 71 infection in mice *J. Virol.* **81** 10310–5
[34] Xu F H *et al* 2010 Performance of detecting IgM antibodies against Enterovirus 71 for early diagnosis *PLoS One* **5** e11388